Performance of a real-time atmospheric turbulence compensation methodology operating on aberrations modeled with Von Karman statistics

T. Coon[1], W. Arrasmith[2]
[1]Florida Institute of Technology, Melbourne, FL, USA tcoon2016@my.fit.edu
[2]Florida Institute of Technology, Melbourne, FL, USA, warrasmi@fit.edu, 321-674-8818

Received: 4 June 2021; **Accepted:** 18 June 2021; **Published:** 21 June 2021

Citation: T. Coon[1], W. Arrasmith [2]. Performance of a real-time atmospheric turbulence compensation methodology operating on aberrations modeled with Von Karman statistics: 47-54.

ABSTRACT

The Well Optimized Linear Finder (WOLF) method is a novel, non-iterative deconvolution method implemented to correct atmospheric and system phase disturbances in optical systems using diversity-based incoherent image irradiance data. The WOLF method addresses the problem of turbulent atmosphere limiting spatial resolution for long-range optical imaging systems having sufficiently large entrance pupil plane apertures such as those in telescopic imaging systems, especially in real-time operation. Developed by Dr. William Arrasmith at the Florida Institute of Technology, the WOLF method exploits symmetries and entrance pupil plane phase redundancies in the discrete convolution of the generalized pupil function to estimate the optimal Optical Transfer Function (OTF). Simultaneously, entrance pupil plane phase disturbances due to the atmospheric aberrations are estimated and used to point-wise estimate the aberration-free object radiant emittance. The sub-algorithms use a novel error metric for generating estimates in the WOLF method. Herein is a qualitative and quantitative investigation in application of the Von Karman stochastic definition to generate representative discrete atmospheric-turbulence-induced phase aberrations for simulated diversity images of an incoherent optical imaging system as input to WOLF method simulations. The Von Karman stochastic definition has advantage over Kolmogorov models in its ability to represent a larger range of atmospheric scale lengths. We also include the effects of optical system noise with addition of Gaussian white noise to demonstrate the efficacy of the WOLF method in application to real-world atmospheric turbulence compensation (ATC).

INTRODUCTION

Performance of terrestrial high-powered optical telescopes is severely limited by the effects of atmospheric turbulence. Traditional Adaptive Optics (AO) and Atmospheric Turbulence Compensation (ATC) methods have enabled correction of the spatial resolution-degrading effects by implementation of adaptive optics and/or post-processing methods. However, many of these solutions are impractical to some degree or other. The adaptive optics solutions operate on real-time signals, but require heavy and complex actuators, limiting the mobility of the solution. The post-processing methods require little additional hardware, but rely on computationally intense algorithms requiring minutes to hours of processing time.[2,7] A solution to this problem enabling ATC in many practical applications is found in the novel WOLF method which reduces post-processing times significantly to enable real-time imaging in a variety of applications and still maintains the mobility of a passive optical system.[1,7] This work investigates the implementation of the WOLF method to simulations with turbulence defined by the Von Karman spectrum.

The effect of atmospheric turbulence on optical propagation has been studied by many mathematicians in

the 20th century. [2, 8] From their works, we have a number of stochastic models which enable the simulation of atmospheric effect on the optical wave front. Implementation of these simulations is imperative to effective adaptive optics hardware and atmospheric turbulence compensation algorithm design. The WOLF method is among those benefitting from exhaustive research into the simulation of atmospheric turbulence. In the work by Arrasmith, the WOLF method is applied to a phase screen realized from the Kolmogorov model using Zernike polynomials. [1] The investigation herein instead builds the phase screen using the Von Karman model and dirac delta basis functions. The Von Karman model of phase effects resulting from the atmosphere can represent many scenarios and has been successfully implemented in industry. [3] It has advantage over other widely used models in its applicability to a greater range of turbulence scale lengths. [2]

To perform the investigation, we generate a realization of the wave front from Von Karman statistics, introduce noise to represent that of a real system, and use it as an input for the optical simulation on which the WOLF method operates. Because the WOLF method estimates the phase exactly at a point, the estimation is anticipated to be valid for the Von Karman simulation as it was for the Kolmogorov simulation.

ANALYSIS

Von Karman turbulence is modeled using the common approach of phase screens. [3] In this approach, the effects of index of refraction variations of the atmosphere are represented by phase offset maps in numerous planes perpendicular to the propagation direction in between the object and entrance pupil, each phase screen accounting for the effects of a corresponding fraction of the propagation path. The Von Karman spectrum is represented at each phase screen by second-order statistics. Each of these phase screens can be combined into a single phase screen in the entrance pupil. To implement Von Karman's work in a digital simulation, it is necessary to discretize the equations for second-order statistics. It is assumed the wave front phase has Gaussian statistics and the amplitude effects of the turbulence are negligible. This is the case for near-field atmospheric turbulence conditions such as ground to air or space imaging systems. The development below results in phase correlations having simple, closed-form expressions. Start with a generic weighted orthonormal basis function representation of the phase screen, Equation (1). [2]

$$\tilde{\psi}(\boldsymbol{x}, t_q) = \sum_{p=1}^{P} a_p(t_q) f_p(\boldsymbol{x}) \quad q = 1, 2, \ldots, Q \tag{1}$$

$\tilde{\psi}$ ≡ Single realization of the phase
$\boldsymbol{x}$ ≡ Pupil position vector
t ≡ Time
f_p ≡ p^{th} – member of a set of orthonormal basis functions
$a_p(t_q)$ ≡ p^{th} – weight for the q^{th} time instant
P ≡ Number of basis functions
Q ≡ Number of instants in time

The goal is to make random draws of weights such that the spatial and temporal correlations and point statistics are characteristic of the atmosphere. The correlation of the phase is defined in Equation (2).

$$\Gamma_{\tilde{\psi}}(\boldsymbol{x}_1, t_q; \boldsymbol{x}_2, t_{q'}) = \mathrm{E}\left[\tilde{\psi}(\boldsymbol{x}_1, t_q)\tilde{\psi}(\boldsymbol{x}_2, t_{q'})\right] \tag{2}$$

$\Gamma_{\tilde{\psi}}$ ≡ Covariance of the phase random process
$\tilde{\psi}$ ≡ Random phase process approximation
$\boldsymbol{x}_1, \boldsymbol{x}_2$ ≡ Positions in the aperture
$t_q, t_{q'}$ ≡ Time instants
q, q' ≡ Time indices $1, 2, \ldots, Q$

This covariance of the random process, $\tilde{\psi}$, is translated to the covariance of the weighted orthonormal basis

function weights, $a_p(t_q)$. To find the weights of the function, project the process function onto the basis functions. [2]

$$a_i = \int d\xi \; W(\xi)\widetilde{\psi}(\xi) f_i(\xi) \tag{3}$$

$$\xi = \begin{bmatrix} \boldsymbol{x}_p \\ t_q \end{bmatrix} \tag{4}$$

Using this definition, find an expression for the covariance of the weights in terms of the process approximated by the weighted orthonormal basis function, $\widetilde{\psi}$. We find the covariance of the weights has a straightforward relationship to the covariance of the process, Equation (5).

$$\begin{aligned} \Gamma_a &= \mathrm{E}\left[a_p(t_q)\, a_{p'}(t_{q'})\right] \\ &= \mathrm{E}\left[\int d\xi \; W(\xi)\widetilde{\psi}(\xi) f_i(\xi) \int d\xi' \; W(\xi')\widetilde{\psi}(\xi') f_j(\xi')\right] \\ &= \int d\xi \int d\xi' \; W(\xi)W(\xi') f_i(\xi) f_j(\xi') \, \mathrm{E}\left[\widetilde{\psi}(\xi)\, \widetilde{\psi}(\xi')\right] \end{aligned} \tag{5}$$

Now, choose the basis functions, in Equation (1). Common choices are the dirac delta functions or Zernike polynomials. Here, we use the dirac delta functions as our basis set. For this development, it is assumed the dirac delta functions exist at the center of each pupil plane grid square and are the same height of the phase offset perpendicular to the pupil plane at the respective point. The dirac delta functions are given by Equation (6).

$$f_p(\boldsymbol{x}) = \delta(\boldsymbol{x} - \boldsymbol{x}_p) \tag{6}$$

Substitution of the dirac delta function, Equation (6), into the covariance expression in Equation (5) yields Equation (7).

$$\begin{aligned} \Gamma_a &= \mathrm{E}\left[a_p(t_q)\, a_{p'}(t_{q'})\right] \\ &= \mathrm{E}\left[\int d\boldsymbol{x} \; W(\boldsymbol{x})\widetilde{\psi}(\boldsymbol{x}, t_q) f_p(\boldsymbol{x}) \int d\boldsymbol{x}' W(\boldsymbol{x}')\widetilde{\psi}(\boldsymbol{x}', t_{q'}) f_{p'}(\boldsymbol{x}')\right] \\ &= \int d\boldsymbol{x} \int d\boldsymbol{x}' \; W(\boldsymbol{x})W(\boldsymbol{x}') f_p(\boldsymbol{x}) f_{p'}(\boldsymbol{x}') \, \mathrm{E}\left[\widetilde{\psi}(\boldsymbol{x}, t_q)\widetilde{\psi}(\boldsymbol{x}', t_{q'})\right] \\ &= \int d\boldsymbol{x} \int d\boldsymbol{x}' \; W(\boldsymbol{x})W(\boldsymbol{x}')\delta(\boldsymbol{x} - \boldsymbol{x}_p)\delta(\boldsymbol{x}' - \boldsymbol{x}_{p'}) \, \mathrm{E}\left[\widetilde{\psi}(\boldsymbol{x}, t_q)\widetilde{\psi}(\boldsymbol{x}', t_{q'})\right] \end{aligned} \tag{7}$$

It is important to note, when using the dirac delta function basis, we must change the definition of the aperture function, $W(\bar{x})$. For the Zernike polynomials, the aperture function is normalized so the integrated area inside the aperture is equal to unity. For the dirac delta basis, the value of the aperture function is unity at each point. With this established, we arrive at the simplification of Equation (9), the covariance of the phase points is the same as the covariance of the weights because the weights are equivalent to the phases when using the dirac delta basis.

$$\mathrm{E}\left[a_p(t_q)\, a_{p'}(t_{q'})\right] = \mathrm{E}\left[\widetilde{\psi}(\boldsymbol{x}_p, t_q)\, \widetilde{\psi}(\boldsymbol{x}_{p'}, t_{q'})\right] \tag{8}$$

$$\Gamma_a(t_q, t_{q'}) = \Gamma_{\widetilde{\psi}}(\boldsymbol{x}_p, t_q; \boldsymbol{x}_{p'}, t_{q'}) \tag{9}$$

The development in Roggemann and Welsh for the covariance expression of the Von Karman spectrum in the pupil plane, including the effects of multiple phase screens, leads to Equation (10).

$$\Gamma_{\phi}(\boldsymbol{x}_p, t_q ; \boldsymbol{x}_{p'}, t_{q'}) = 3.089\left(\sum_{i=1}^{N} r_{0_i}^{-5/3} \int_0^{\infty} \kappa \, d\kappa \, J_0(\kappa \, \rho)\Phi_0^V(\kappa)\right) \tag{10}$$

$$\Phi_0^V(\kappa) = \frac{1}{\left(\kappa^2 + 4\pi^2/L_0^2\right)^{11/6}} \tag{11}$$

$$\rho = \left|\boldsymbol{x}_p - \boldsymbol{x}_{p'} - \boldsymbol{v}\left(t_q - t_{q'}\right)\right| \tag{12}$$

ϕ ≡ Combined phase screen in the entrance pupil
Γ_{ϕ} ≡ Covariance expression for phase in the entrance pupil
N ≡ Number of layers (phase screens)
r_{0_i} ≡ Coherence length of layer i
κ ≡ Wavenumber
J_0 ≡ Zeroth – order Bessel function of the first kind
ρ ≡ Radial separation between two field points
$\boldsymbol{v}$ ≡ Wind velocity vector
Φ_0^V ≡ Normalized spectral density, Von Karman
L_0 ≡ Outer scale length of atmospheric turbulence

From this point, we consider two cases. In the first case, $\rho \neq 0$ and the integral is reduced to the closed form of Equation (13). [2]

$$\int_0^{\infty} \kappa \, d\kappa \, J_0(\kappa \, \rho)\left(\kappa^2 + 4\pi^2/L_0^2\right)^{-11/6} = \frac{(L_0/2\pi)^{5/6} K_{5/6}[2\pi\rho/L_0]\rho^{5/6}}{2^{5/6}\Gamma[11/6]} \tag{13}$$

$K_{5/6}[\cdot]$ ≡ Modified Bessel function of the second kind of order $5/6$
$\Gamma[\cdot]$ ≡ Gamma function

However, we found this solution to be insufficient because $\rho = 0$ causes $K_{5/6}[0] = \infty$ in Equation (13). This necessarily occurs in calculation of the variance. As such, we must consider a second case in which the argument of the Zeroth-order Bessel function of the first kind in Equation (10) is zero, so $J_0(0) = 1$. We solved for the closed-form solution in this case, Equation (14).

$$\int_0^{\infty} \kappa \, d\kappa \left(\kappa^2 + 4\pi^2/L_0^2\right)^{-11/6} = \frac{3}{5(2\pi/L_0)^{5/3}} \tag{14}$$

Notice, the machine precision of the computer can lead to a covariance matrix having eigenvalues which are less than zero by some small value. Modify Γ_{ϕ} so each of its eigenvalues is nonnegative by first assuring all negative eigenvalues are indeed small, then, setting each eigenvalue below a certain threshold value to zero. The new semi-positive definite covariance matrix is generated from the corrected eigenvalues and the original eigenvectors using the formula in Equation (15). [10]

$$A_{pd} = \nu \, D_c \, \nu'$$

A ≡ Original matrix
A_{pd} ≡ Positive definite matrix
ν ≡ Column matrix of eigenvectors of A
D_c ≡ Diagonal matrix with corrected eigenvalues

(15)

We now have the matrix expression for the covariance of the phase at points in the entrance pupil induced by atmospheric turbulence. To generate a realization of the phase in the entrance pupil for the simulation, use the procedure detailed in Brown & Hwang.[4] The Singular Value Decomposition (SVD) of Γ_{ϕ} is found using the

$$U = V^T$$

$$\boldsymbol{a}$$

$$\Gamma_{\phi}$$

svd () function in MATLAB®. Notice Brown & Hwang use different notation and definitions than MATLAB®.[13] Because Γ_ϕ is symmetric, . Using quantities from the SVD of the covariance of the phase, Γ_ϕ, a realization of the weights, , for the phase expression of Equation (1) is generated which have a Gaussian distribution and covariance, . Because we used the dirac delta basis functions, these coefficients are exactly a realization of the phase at each point in the entrance pupil.

$$[U,\ T,\ V] = \text{svd}(Q) \tag{16}$$

$$\boldsymbol{a} = U\sqrt{T}\,u \tag{17}$$

$$u \sim N(0,1) \tag{18}$$

$U \equiv$ Left singular vectors
$V \equiv$ Right singular vectors
$T \equiv$ Matrix with singular values on the diagonal
$\boldsymbol{a} \equiv$ Vector of weights of the phase expression

After generating the phase in the entrance pupil plane, the generalized pupil function (GPF) is found by applying Equation (19) at every sample point in the entrance pupil plane of the imaging system.

$$W(\boldsymbol{x}) = A(\boldsymbol{x})e^{j\phi(\boldsymbol{x})} \tag{19}$$

$W(\boldsymbol{x}) \equiv$ Generalized pupil function (GPF)
$A(\boldsymbol{x}) \equiv$ Aperture function
$\phi(\boldsymbol{x}) \equiv$ Phase at $\boldsymbol{x}$ in the entrance pupil plane

Equation (20) is then applied to find the Optical Transfer Function (OTF). Where ⊗ is the autocorrelation operation and the spatial position is related to the spatial frequency by input wavelength and system geometry. [2]

$$\mathscr{H}(\boldsymbol{f}) = \frac{W(\boldsymbol{x}) \otimes W(\boldsymbol{x})}{W(\boldsymbol{0}) \otimes W(\boldsymbol{0})} \tag{20}$$

$\mathscr{H}(\boldsymbol{f}) \equiv$ Optical Transfer Function
$\boldsymbol{f} \equiv$ Spatial Frequency Vector

The OTF is necessary in the simulation to generate the aberrated images which are used as inputs to the WOLF method. To generate the aberrated images, the Truth Object is Fourier transformed to produce the Object Spectrum and multiplied, point-wise, with the OTF to form the Image Spectrum. These operations in Fourier space are given by Equation (21).

$$I(\boldsymbol{f}) = O(\boldsymbol{f})\mathscr{H}(\boldsymbol{f}) \tag{21}$$

$I(\boldsymbol{f}) \equiv$ Image Spectrum
$O(\boldsymbol{f}) \equiv$ Object Spectrum

The Image is then generated from the Image Spectrum by the 2D inverse Fourier transform. In the next section, we present our results.

RESULTS

We illustrate the application of the WOLF method to simulations with a Von Karman turbulence model using a 256 x 256 pixel image of Saturn taken by the Wide Field Camera 3 (WFC3) on the Hubble Space

Telescope.[9] This is assumed to be a pristine image and has been converted to grayscale in MATLAB® using rgb2gray().[13] The imaging system parameters and image characteristics were investigated to assure the image is a subset of the real image and had not been scaled. Using imresize() in MATLAB®, the image was reduced to 256 x 256 pixels. To simulate the image as if it were captured from the earth's surface, Von Karman turbulence is added according to the method of the previous section of this paper. We use a square entrance pupil plane with 127 x 127 samples. This leads to an image and OTF which are each 256 x 256. The truth radiant emittance of the unaberrated object is shown in Figure 1.

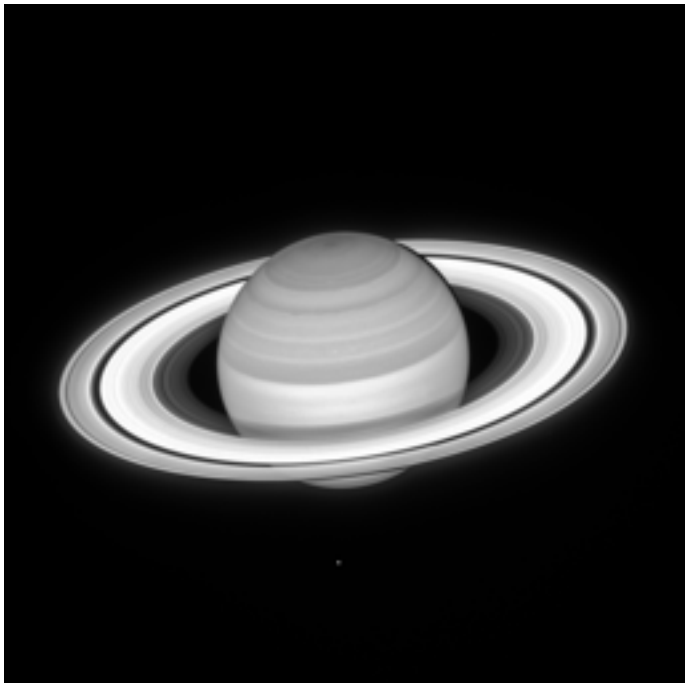

Figure 1 – Truth Radiant Emittance (Truth Object) [9]

The Truth Object shows the detail of Saturn with clear ring lines and one of the moons is visible at the bottom of Figure1. Both this Image and a Diversity Image generated from a known offset of the phase are the image pair, along with imaging system parameters, then supplied as inputs to the WOLF method.

Using the Von Karman spectrum and the simulation method detailed above, a realization of the phase in the entrance pupil is generated. Remember, these phases are defined point-wise because the weights in Equation (1) are exactly the phase offset at each pupil plane point. An example realization of the Von Karman simulated entrance pupil plane phases with zero-mean, Gaussian noise added are shown in Figure 2.

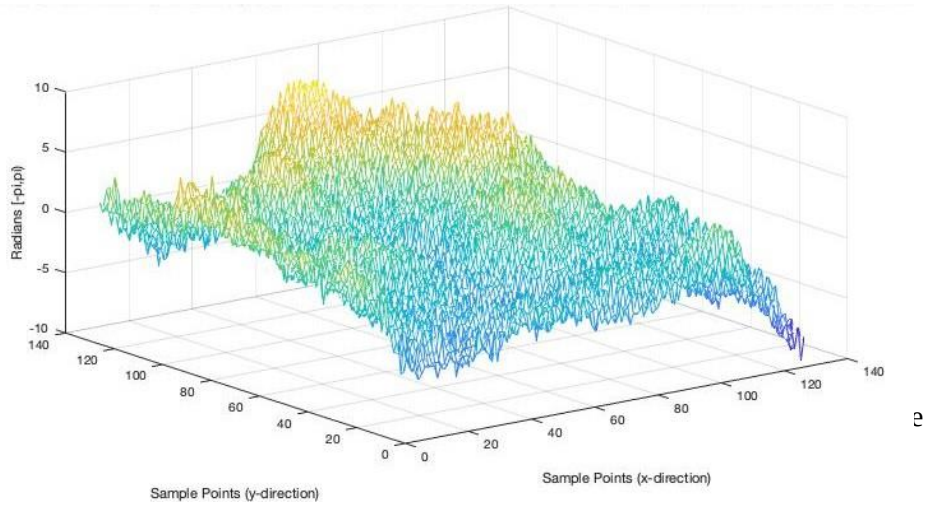

Figure 2 - Entrance Pupil Plane Generated Phase Realization with Von Karman Atmospheric Statistics

The corresponding modulation transfer function (MTF) is shown in Figure 3. The noticeable departure from a diffraction-limited MTF indicates the turbulence this simulated system is subjected to is severe.

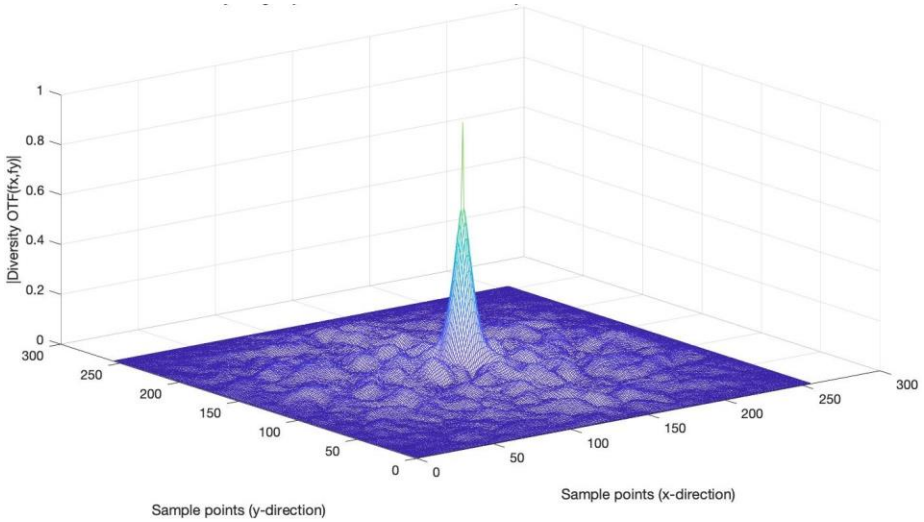

Figure 3 – Modulation Transfer Function

Multiplication of the Object Spectrum and the Optical Transfer Function generate the Aberrated Image Spectrum which is 2D inverse Fourier transformed to find the simulated Aberrated Image shown in Figure 4. The realization of Von Karman turbulence in the simulation severely degrades the resolution of the Truth Object so the separate rings and the moon are no longer distinguishable.

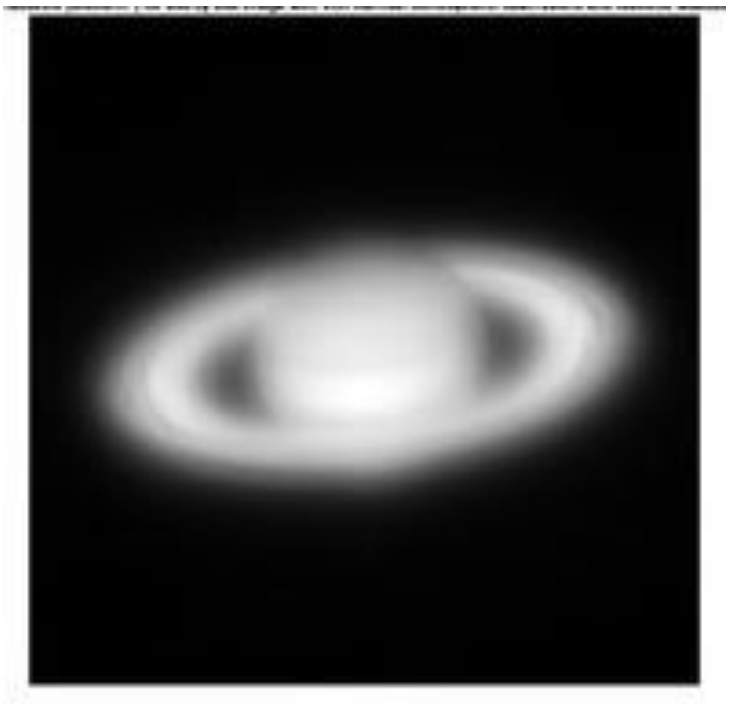

Figure 4 - Aberrated Image

Applying the WOLF method, the degrading effects of the atmosphere are removed, resulting in the

Reconstructed Image shown in Figure 5. This estimated image is indistinguishable from the Truth Object and shows the efficacy of the WOLF method operating on strong turbulence with Von Karman covariance and Gaussian noise.

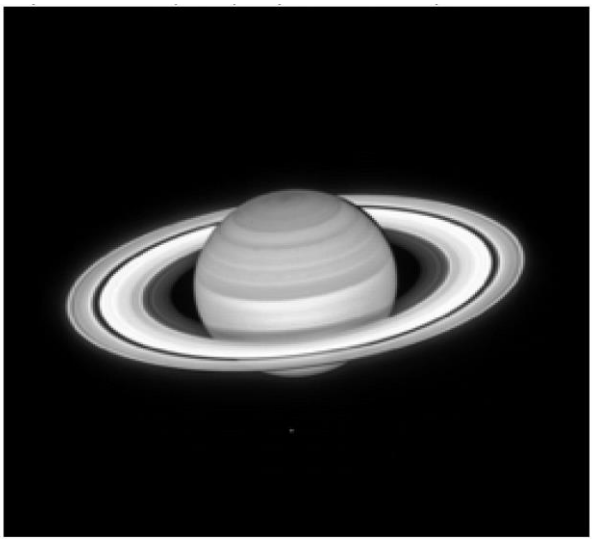

Figure 5 - Reconstructed Object Radiant mittance

CONCLUSION

This research set out to investigate the performance of the WOLF method in removing the effects of atmospheric turbulence simulated using the Von Karman spectrum. The process for simulating a phase screen realization was detailed with traceability to show it characterized the Von Karman power spectrum definition of the atmospheric turbulence. Using this process, the optical phase offset in the entrance pupil induced by turbulence was simulated for a single instant in time. This phase generated an aberrated image as would be captured by a conventional terrestrial imaging system. Generating a diversity image as well and submitting these as inputs to the WOLF method resulted in a Reconstructed Image which is indistinguishable from the Truth Object. This simulation proves the WOLF method can be effective when used to remove aberrations simulated using the Von Karman definition of turbulence. It is important to note, the same covariance expression is used to link multiple phase screens in time.

REFERENCES

1. W. Arrasmith, 2021. In press, Diversity-based atmospheric turbulence compensation for incoherent imaging systems using a new well optimized linear finder methodology. Unpublished Article. Submitted for publication.
2. M. C. Roggemann, B. Welsh, *Imaging Through Turbulence*, CRC Press, New York, 1996.
3. T. Goldring and L. Carlson., "Analysis and implementation of non-kolmogorov phase screens appropriate to structured environments," in *SPIE proceedings on Nonlinear Optical Beam Manipulation and High Energy Beam Propagation Through the Atmosphere*, vol. 1060, pp. 244-264, 1989
4. R.G. Brown and P.Y. Hwang, Introduction to Random Signals and Applied Kalman Filtering With MATLAB Exercises©, 4th ed. Wiley and Sons, Inc., Hoboken, NJ, 2012.
5. J.W. Goodman, *Introduction to Fourier Optics*, McGraw-Hill, New York, 1968.
6. J.W. Goodman, *Statistical Optics*, Wiley and Sons, Inc., New York, 1985.
7. W.W. Arrasmith, "High-speed Diversity-based Imaging Method for Parallel Atmospheric Turbulence Compensation," U.S. patent number: US 8,447,129 B2, May 21, 2013.
8. V.I. Tatarskii, *Wave Propagation in a Turbulent Medium*. New York: Dover Publications, 1967.
9. Space Telescope Science Institute. 23 July, 2020. Hubblesite. https://hubblesite.org/image/4713/gallery
10. E. Kreyszig, *Advanced Engineering Mathematics*, 10th ed., Wiley and Sons, Inc., Hoboken, NJ, 2011.
11. A. Papoulis, *Probability Random Variables, and Stochastic Processes*. New York: McGraw-Hill, third ed., 1991.
12. A. Ishimaru, *Wave Propagation and Scattering in Random Media*, vol. 2. New York Academic Press, 1978
13. MATLAB version 9.7.0 Natick, Massachussettes: Mathworks, Inc., 2019